Electron-Phonon Interaction and Transport in Semiconducting Carbon Nanotubes

Vasili Perebeinos, J. Tersoff, and Phaedon Avouris*

IBM Research Division, T. J. Watson Research Center, Yorktown Heights, New York 10598, USA

(Received 29 October 2004; published 2 March 2005)

We calculate the electron-phonon scattering and binding in semiconducting carbon nanotubes, within a tight-binding model. The mobility is derived using a multiband Boltzmann treatment. At high fields, the dominant scattering is interband scattering by LO phonons corresponding to the corners K of the graphene Brillouin zone. The drift velocity saturates at approximately half the graphene Fermi velocity. The calculated mobility as a function of temperature, electric field, and nanotube chirality are well reproduced by a simple interpolation formula. Polaronic binding give a band-gap renormalization of $\sim$70 meV, an order of magnitude larger than expected. Coherence lengths can be quite long but are strongly energy dependent.

DOI: 10.1103/PhysRevLett.94.086802 PACS numbers: 73.63.Fg, 72.10.Di, 85.35.Kt

Carbon nanotubes have enabled novel electronic devices, including quasi-one-dimension field-effect transistors [1] and electro-optical devices [2,3]. Much effort has gone into determining the transport properties, which are crucial for these and other applications. Nanotubes exhibit high mobility at low electric fields, exceeding the best semiconductors at room temperature [4]. At high fields, the mobility is dramatically reduced by optical phonon emission, leading to interesting saturation behavior [5–7]. However, little is known about how the mobility varies with temperature, electric field, and tube diameter and chirality.

Here we calculate the electron-phonon interactions and drift velocity in semiconducting nanotubes, within a standard tight-binding approach. Our results are consistent with available measurements, and provide a detailed microscopic picture of phonon scattering. For example, we find that there is a broad maximum in coherence length at intermediate energies, centered at 100–150 meV, with coherence lengths of over a micron at room temperature, and much larger at low temperature. At large fields, the mobility is limited primarily by interband scattering from the LO phonons corresponding the corners of the graphene Brillouin zone.

At the same time, we provide a broad overview of the transport, by calculating the mobility over a wide range of temperature, electric field, and nanotube structure. The low-field mobility depends strongly on nanotube diameter and temperature, while at high field the drift velocity approaches a roughly universal value. We show that these dependences can be well described by a simple formula.

In addition, we find that polaronic binding gives a significant band-gap renormalization, reducing the gap by around 70 meV over a range of tube diameters. This is more than an order of magnitude larger than suggested by previous calculations [8,9], and is particularly important for larger-diameter tubes, where it represents a significant fraction of the band gap.

Our calculations use a standard tight-binding description for the electronic structure [10]. The phonons are described using an improved model somewhat similar to that of Aizawa *et al.* [11]. We model the electron-phonon (e-ph) interaction by the Su-Schrieffer-Heeger (SSH) model [12], with matrix element $t = t_0 - g\delta u$ dependent on the change of the nearest neighbor C-C distance (δu), where $t_0 = 3$ eV. We take the e-ph coupling constant to be $g = 5.3$ eV/Å [13,14]. The Fourier transformed SSH Hamiltonian here is

$$\mathcal{H}_{e-ph} = \sum_{kq\mu} \mathrm{M}^{\mu}_{kq} (v^{\dagger}_{k+q} v_k - u^{\dagger}_{k+q} u_k)(a_{q\mu} + a^{\dagger}_{-q\mu}), \quad (1)$$

where $\mathrm{M}^{\mu}_{kq} \propto gN^{-1/2}$ is the e-ph coupling [15], $u^{\dagger}_{k+q}(v_k)$ denotes creation (annihilation) of an electron in the conduction (valence) band, $a^{\dagger}_{-q\mu}$ is a phonon creation operator with wave vector $-q$ and phonon band index $\mu = 1 \ldots 6$, and N is the number of the primitive unit cells each containing two carbons. The indices k and q each label both the continuous wave vector along the tube axis and the discrete circumferential wave vector.

We consider a single electron in the conduction band; the behavior of a single hole would be identical. The charge carrier with wave vector k and energy ε_k can be scattered to a state with wave vector $k + q$ by absorbing (emitting) a phonon with wave vector q $(-q)$, and having energy $\hbar\omega_q (= \hbar\omega_{-q})$ such that the net momentum and energy are conserved.

The scattering rate for an electron of wave vector k, in the random phase approximation, is

$$\frac{1}{\tau_k} = \sum_q W_{k,k+q},$$

$$W_{k,k+q} = \frac{2\pi}{\hbar} \sum_{\mu} |M^{\mu}_{k,q}|^2 [n_{q\mu}\delta(\varepsilon_k - \varepsilon_{k+q} + \hbar\omega_{q\mu}) + (1 + n_{-q\mu})\delta(\varepsilon_k - \varepsilon_{k+q} - \hbar\omega_{-q\mu})], \quad (2)$$

where τ_k is the scattering time, and the phonon occupation number $n_{q\mu}$ is given by the Bose-Einstein distribution. The energy shift due to electron-phonon coupling is

$$\delta E_k = \mathrm{Re}\sum_{q\mu}|M^{\mu}_{kq}|^2\left[\frac{n_{-q}+1}{\varepsilon_k-\varepsilon_{k+q}-\hbar\omega_{-q\mu}-i\delta} + \frac{n_q}{\varepsilon_k-\varepsilon_{k+q}+\hbar\omega_{q\mu}-i\delta}\right], \quad (3)$$

in the limit $\delta \to 0$.

The results for the binding energy and the scattering rate of a charge carrier in the first band are shown in Fig. 1 for a tubes of diameter $d = 2.0$ nm. The binding energy in Fig. 1(a) is nearly independent of temperature over the entire energy range, and only weakly energy dependent at low energy. The binding energy increases sharply at resonance with the optical phonon K_{LO}. The scattering rate (inverse lifetime) in Fig. 1(b) shows a strong temperature dependence at low energy, but at high energy it is 2 orders of magnitude larger and nearly independent of temperature.

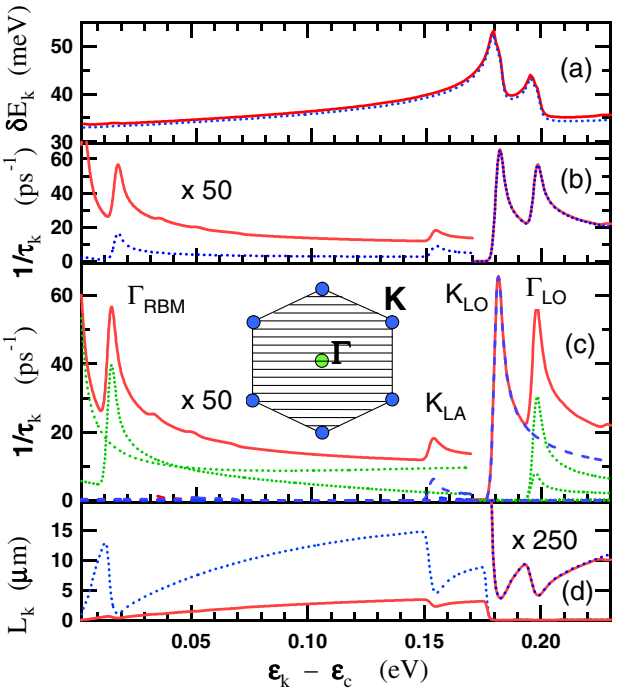

FIG. 1 (color online). Phonon binding and scattering vs electron energy ε_k (relative to conduction band edge ε_c), for a (25,0) tube ($d = 2.0$ nm). (a) Binding energy, Eq. (3); (b-c) inverse lifetime, Eq. (2); and (d) coherence length. The energy range shown includes only the first band. In (a), (b), and (d), solid red curves are for $T = 300$ K, dotted blue curves are for $T = 10$ K. Note the large change in scale between low and high energy [$\times$ 50 in (b) and (c) for low energy, and $\times$250 in (d) for high energy]. (c) Decomposition of *e-ph* scattering rate for 300 K: total (red solid curve); Γ-point contributions (green dotted curves); K-point contributions (blue dashed curves). Γ_{RBM} is radial breathing mode. The inset shows 2D graphene Brillouin zone, with the integration areas shown by the circles of radius equal to 0.1 of the Γ–M distance, which contribute virtually 100% of the total scattering; lines are only schematic.

Virtually all of the scattering is by phonons corresponding to small regions near the Γ and K points of the 2D graphene Brillouin zone, and Fig. 1(c) shows the contributions of the respective bands to the scattering. At low electron energy, the scattering is by acoustic and breathing-mode phonons near the Γ point. The lowest-energy phonon band gives negligible scattering and is not shown. The second band is the acoustic phonon contribution which peaks at the van Hove singularity (bottom of the conduction band). The third band is the radial breathing mode [at 15 meV in (25,0) tube]. The next phonon mode with a nonnegligible *e-ph* coupling is the longitudinal acoustic phonon at K point which gives a weak scattering peak labeled K_{LA}.

By far the strongest coupling is to the LO phonons, which give scattering roughly 2 orders of magnitude stronger than the acoustic modes. The K_{LO} mode corresponds to interband scattering. It is the most important mode at high field, both because it is strongest, and because it can scatter electrons before they reach the energy of the Γ_{LO} mode.

In Fig. 1(d) we show the coherence length, defined as $L_k = v_k\tau_k$, where v_k is the band velocity. (We neglect phonon renormalization of v_k, which we calculate to be only a few percent except near resonance with the optical phonons K_{LO} and Γ_{LO}.) Note that the coherence length is strongly energy dependent, with a broad maximum between the breathing mode and the optical phonons. It is also quite sensitive to temperature, but even at room temperature the coherence length can be well over a micron, consistent with lengths inferred from experiment [6,7]. Charge carriers can be injected into nanotubes well above the band edge [16], suggesting the possibility of ballistic or even quantum-coherent devices over a range of length scales. At higher energy, the carriers have a temperature independent coherence length of around 20–40 nm, depending on energy. This is consistent with the lengths inferred from experiments for metallic tubes [5–7].

For applications such as diffusive device modeling, what is needed is the total effect of scattering on the transport. This is expressed as a mobility, which we calculate by solving the steady-state multiband Boltzmann equation in the presence of an electric field. The electron momentum distribution function g_k is

$$\frac{eE}{\hbar}\frac{\partial g_k}{\partial k} = -\sum_q [W_{k,k+q}g_k(1-g_{k+q}) - W_{k+q,k}g_{k+q} \times (1-g_k)], \quad (4)$$

where $W_{k,k+q}$ is given in Eq. (2). Using the nonequilibrium distribution function g_k from Eq. (4), we calculate the drift velocity v and the mobility μ. To model nonuniform fields or partially ballistic regimes, one can perform Monte Carlo simulations using the full scattering matrix $W_{k,k+q}$.

The drift velocity versus E field is shown in Fig. 2(a), for a (25,0) tube. We show results at room temperature and at low temperatures, in the limit of low carrier density. The drift velocity saturates for fields $E \gtrsim 0.5$ V/μm. At low temperature we find negative differential resistance, i.e., drift velocity decreasing with increasing field. A similar observation was reported previously [17], and it was speculated to result from population of the second band at high field. However, we find that the behavior persists even if we restrict the basis set to include only the first band.

The inverse mobility shown in Fig. 2(b) can be fitted rather well by a simple linear function of the E field, over a wide range of applied E fields:

$$\mu^{-1} \approx \mu_0^{-1} + v_s^{-1} E, \tag{5}$$

where μ_0 is the zero-field mobility and v_s is the saturation velocity. This is analogous to the linear dependence $R = R_0 + V/I_0$ found for the dependence of the resistance R of metallic nanotubes with applied voltage V [5], where I_0 is a saturation current. The saturation drift velocity $v_s \approx 5.0 \pm 0.3 \times 10^7$ cm/s is nearly independent of the tube diameter and temperature. The lack of strong dependence on diameter is perhaps surprising, but this velocity is intriguingly close to half of the maximum band velocity (the Fermi velocity of graphene, 9.8×10^7 cm/s for the value of the tight-binding matrix element t used here).

One of the greatest obstacles to fabricating reproducible nanotube devices, is the difficulty of controlling (or even knowing) the tube structure. This structure, the diameter and chirality, is specified by two indices (m, n). In Fig. 3(a), we show how the zero-field mobility depends on tube structure. We find that the dependence on diameter and temperature can be described by a single simple empirical relation:

$$\mu_0(T, d) = \mu_1 \frac{300\ \mathrm{K}}{T} \left(\frac{d}{1\ \mathrm{nm}} \right)^{\alpha}, \tag{6}$$

with $\mu_1 = 12\,000$ cm^2/Vs and $\alpha = 2.26$. (The arbitrary constants 300 K and 1 nm are simply to give μ_1 units of mobility, independent of α.) The structure dependence is not entirely captured by the diameter, nor is the $1/T$ temperature dependence very precise, but overall the agreement is quite good. Thus the dependence of mobility on temperature, field strength, and even nanotube structure can be captured to useful accuracy ($\sim$10%) with a simple three-parameter description, Eqs. (5) and (6).

It might seem surprising that, while the scattering in Fig. 1 is strongly energy dependent, the mobility in Fig. 2 varies smoothly with increasing field. This can be understood by considering the distribution function g_k [or equivalently g_E] obtained by solving the Boltzmann equation. This is shown in Fig. 4. At very low field, the scattering is entirely by acoustic phonons, giving a smooth distribution in k. (The distribution in energy reflects the van Hove singularity in the density of states.) With increasing field, the electron has an increasing probability of reaching the

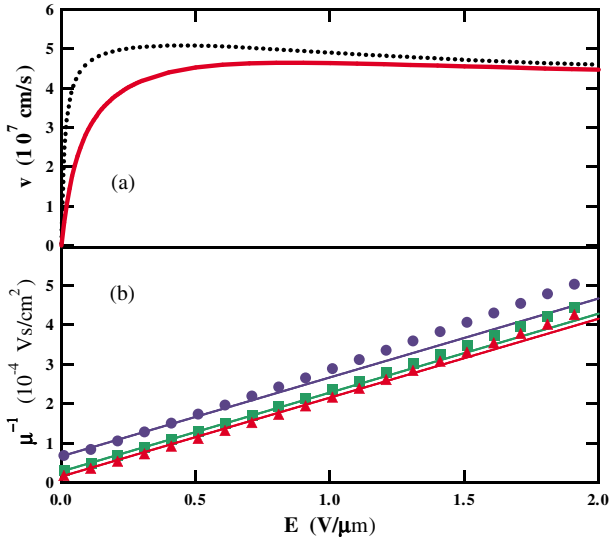

FIG. 2 (color online). (a) Drift velocity vs electric field at $T = 300$ K (red solid curve) and $T = 10$ K (black dotted curve) in (25,0) tube. (b) Inverse mobility at $T = 300$ K vs E field; straight lines show corresponding fits to Eq. (5), with $v_s = 5.0 \times 10^7$. Fitted values of μ_0 are $\mu_0 = 65\,000$ cm^2/Vs for (25,0) tube (red triangles); $\mu_0 = 35\,500$ cm^2/Vs for (19,0) tube (green squares); and $\mu_0 = 15\,000$ cm^2/Vs for (13,0) tube (blue circles).

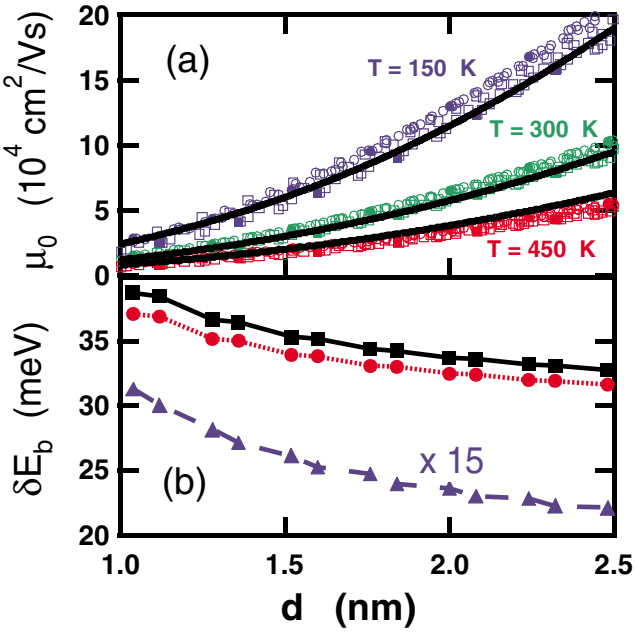

FIG. 3 (color online). (a) Zero-field mobility vs tube diameter, for tubes of many different chiralities. Temperatures are $T = 450$ K (red), $T = 300$ K (green), and $T = 150$ K (blue). Values are based on linear extrapolation of μ^{-1}, Eq. (5), for E field between 0.01 and 0.5 V/μm. Solid black curves are fitted to Eq. (6). (b) Polaron binding energy (black squares) vs tube diameter. Red circles show portion of binding energy from optical phonons, and blue triangles show the much smaller binding energy (shown $\times 15$) from acoustic phonons.

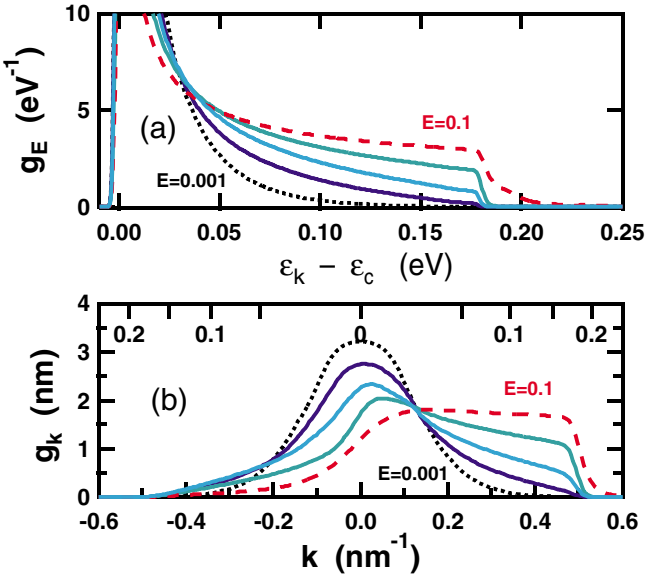

FIG. 4 (color online). Steady-state distribution function for an electron in a (25,0) tube at $T = 300$ K. E fields are $E = 0.001$ V/μm (black dotted curve), 0.01 (blue, next to black dotted curve), 0.03 (light blue, middle), 0.1 (green, next to red dashed curve), and 0.5 (red dashed curve) V/μm. Distributions are shown with respect to (a) energy, and (b) wave vector along tube axis. The top axis in (b) shows corresponding energy. (Curves include Gaussian broadening of 2 meV.)

optical phonon energy, at which point it is quickly scattered. This leads to a step in the distribution near the phonon energy (0.18 eV). With increasing field, the distribution becomes flatter below this energy, until at high field the distribution is almost flat in k, with a sharp step at the phonon energy. From Eq. (5), we might expect the crossover from acoustic to optical phonons as the dominant scattering mechanism to occur roughly at fields $E \sim v_s/\mu_0$, corresponding to $\sim$0.08 V/μm in Fig. 4. This is indeed roughly the field strength where intermediate behavior is seen in g_k. Then from Eqs. (5) and (6), we can anticipate that the crossover field varies with temperature and tube size approximately as $d^{-\alpha}T$.

Finally we return to the polaronic energy shift. Figure 3(b) shows the shift calculated with Eq. (3), as a function of nanotube diameter. [This refers to the band-edge states, $\varepsilon_k = \varepsilon_c$ in Fig. 1(a)] We find binding energies of around 35 meV, with only a weak dependence on diameter over the typical range. This corresponds to a band-gap renormalization of 70 meV due to electron-phonon interactions, which is quite significant for large-diameter tubes. This is more than an order of magnitude larger than previous theoretical estimates [8,9]. The reason for this discrepancy is explained in Fig. 3(b). Previous calculations used a continuum model, which is equivalent to including acoustic but not optical phonons. However, almost all the binding is due to optical phonons, which couple far more effectively to the electrons. If we repeat the calculations using only the first three phonon bands, we obtain only a weak binding, in excellent agreement with continuum calculations [9].

In conclusion, we find that in semiconducting carbon nanotubes, the scattering of electrons or holes by phonons is strongly energy dependent, both at low energy and around the optical phonon energies. Nevertheless, the mobility at low carrier densities can be described fairly accurately by a simple formula, which should be useful in the analysis of nanotube devices. The polaronic binding energy is much larger than expected, giving a significant renormalization of the band gap.

*Electronic address: avouris@us.ibm.com

[1] Ph. Avouris, MRS Bull., **29**, 403 (2004); P. L. McEuen, M. S. Fuhrer, and H. Park, IEEE Trans. Nanotechnol. **1**, 78 (2002); H. J. Dai, Surf. Sci., **500**, 218 (2002).
[2] J. A. Misewich, R. Martel, Ph. Avouris, J. C. Tsang, S. Heinze, J. Tersoff, Science **300**, 783 (2003).
[3] M. Freitag, J. Chen, J. Tersoff, J. C. Tsang, Q. Fu, J. Liu, and Ph. Avouris, Phys. Rev. Lett. **93**, 076803 (2004).
[4] T. Dürkop, S. A. Getty, Enrique Cobas, and M. S. Fuhrer, Nano Lett. **4**, 35 (2004).
[5] Z. Yao, C. L. Kane, and C. Dekker, Phys. Rev. Lett. **84**, 2941 (2000).
[6] A. Javey, J. Guo, M. Paulsson, Q. Wang, D. Mann, M. Lundstrom, and H. Dai, Phys. Rev. Lett. **92**, 106804 (2004).
[7] J. Y. Park, S. Rosenblatt, Y. Yaish, V. Sazonova, H. Ustunel, S. Braig, T. A. Arias, P. Brouwer and P. L. McEuen, Nano. Letters **4**, 517 (2004).
[8] M. Verissimo-Alves, R. B. Capaz, B. Koiller, E. Artacho, and H. Chacham, Phys. Rev. Lett. **86**, 3372 (2001).
[9] E. Piegari, V. Cataudella, V. Marigliano Ramaglia, and G. Iadonisi, Phys. Rev. Lett. **89**, 049701 (2002).
[10] R. Saito and H. Kataura, in *Carbon Nanotubes: Synthesis, Structure, Properties and Application*, edited by M. S. Dresselhaus, G. Dresselhaus, and P. Avouris (Springer-Verlag, Heidelberg, 2001), Vol. 80.
[11] T. Aizawa, R. Souda, S. Otani, Y. Ishizawa, and C. Oshima, Phys. Rev. B **42**, 11 469 (1990); **43**, 12 060(E) (1991).
[12] W. P. Su, J. R. Schrieffer, and A. J. Heeger, Phys. Rev. Lett. **42**, 1698 (1979); Phys. Rev. B **22**, 2099 (1980).
[13] V. Perebeinos, P. B. Allen, and M. Pederson, cond-mat/0208051.
[14] C. R. Fincher, Jr., D. L. Peebles and A. J. Heeger, M. A. Druy, Y. Matsumura, A. G. MacDiarmid, H. Shirakawa, and S. Ikeda, Solid State Commun. **27**, 489 (1978).
[15] G. D. Mahan, Phys. Rev. B **68**, 125409 (2003). Here we neglect terms corresponding to virtual electron-hole excitations across the band-gap.
[16] S. Heinze, J. Tersoff, and Ph. Avouris, Appl. Phys. Lett. **83**, 5038 (2003).
[17] G. Pennington and N. Goldsman, Phys. Rev. B **68**, 045426 (2003).